

Elimination of quiescent/slow-proliferating cancer stem cells by Bcl-X_L inhibition in non-small cell lung cancer

A Zeuner^{*1}, F Francescangeli¹, P Contavalli¹, G Zapparelli¹, T Apuzzo², A Eramo¹, M Baiocchi¹, ML De Angelis¹, M Biffoni¹, G Sette³, M Todaro², G Stassi² and R De Maria³

Lung cancer is the most common cause of cancer-related mortality worldwide, urging the discovery of novel molecular targets and therapeutic strategies. Stem cells have been recently isolated from non-small cell lung cancer (NSCLC), thus allowing the investigation of molecular pathways specifically active in the tumorigenic population. We have found that Bcl-X_L is constantly expressed by lung cancer stem cells (LCSCs) and has a prominent role in regulating LCSC survival. Whereas chemotherapeutic agents were scarcely effective against LCSC, the small molecule Bcl-2/Bcl-X_L inhibitor ABT-737, but not the selective Bcl-2 inhibitor ABT-199, induced LCSC death at nanomolar concentrations. Differently from gemcitabine, which preferentially eliminated proliferating LCSC, ABT-737 had an increased cytotoxic activity *in vitro* towards quiescent/slow-proliferating LCSC, which expressed high levels of Bcl-X_L. *In vivo*, ABT-737 as a single agent was able to inhibit the growth of LCSC-derived xenografts and to reduce cancer stem cell content in treated tumors. Altogether, these results indicate that quiescent/slow-proliferating LCSC strongly depend on Bcl-X_L for their survival and indicate Bcl-X_L inhibition as a potential therapeutic avenue in NSCLC.

Cell Death and Differentiation (2014) 21, 1877–1888; doi:10.1038/cdd.2014.105; published online 18 July 2014

Lung cancer is the leading cause of cancer-related death in men and is expected to become the main cause of cancer death for women in the near future.^{1,2} There is increasing evidence that cancer stem cells (CSCs) have a key role in drug resistance, tumor progression and metastasis in multiple tumor types, including lung cancer.³ Lung cancer stem cells (LCSCs) have been previously identified through different criteria including surface expression of CD133, c-kit or through functional properties such as selective drug survival, elevated aldehyde dehydrogenase (ALDH) activity, increased glycolysis and glycine/serine metabolism or low concentrations of reactive oxygen species and ATP.^{4–9} Importantly, when inoculated into immunocompromised mice, LCSCs give rise to xenografts that histologically reproduce the tumor of origin, thus representing an improved model for *in vivo* testing of new targeted therapies.¹⁰ Several tumors express elevated levels of anti-apoptotic Bcl-2 family proteins such as Bcl-2,

Bcl-X_L and Mcl-1, which affect the apoptotic threshold of neoplastic cells contributing to chemotherapy resistance.¹¹ Inhibition of anti-apoptotic Bcl-2 family members has been for long time regarded as a promising strategy to induce cancer cell death through approaches of increasing specificity. BH3 mimetics such as ABT-737, the related orally available ABT-263 (navitoclax) and the recently developed Bcl-2-selective inhibitor ABT-199 have been shown to exert an antitumor effect in preclinical and clinical settings either as single agents or in combination with conventional or targeted drugs.¹² Recently, a new role for Bcl-2 has emerged in acute myeloid leukemia (AML), where quiescent stem cells characterized by low levels of reactive oxygen species were found to over-express Bcl-2 and rely on this factor for survival.¹³ Similarly, in chronic myeloid leukemia (CML), quiescent therapy-resistant stem cells were sensitized to tyrosine kinase inhibitors by treatment with a pan-Bcl-2 inhibitor.¹⁴ In solid tumors, the role

¹Department of Hematology, Oncology and Molecular Medicine, Istituto Superiore di Sanità, Rome 00161, Italy; ²Department of Surgical and Oncological Sciences, University of Palermo, Palermo 90128, Italy and ³Regina Elena National Cancer Institute, Rome, Italy

*Corresponding author: A Zeuner, Department of Hematology, Oncology and Molecular Medicine, Istituto Superiore di Sanità, Viale Regina Elena 299 Rome 00161, Italy. Tel +39 6 4990 6060; Fax +39 6 4938 7087; E-mail: a.zeuner@iss.it

Abbreviations: NSCLC, non-small cell lung cancer; Bcl-X_L, B-cell lymphoma-extra large; LCSC, lung cancer stem cells; Bcl-2, B-cell lymphoma 2; CSC, cancer stem cell; ALDH, aldehyde dehydrogenase; ATP, adenosine triphosphate; Mcl-1, myeloid-cell leukemia 1; BH3, Bcl-2 homology 3 domain; AML, acute myeloid leukemia; CML, chronic myeloid leukemia; EGF, epidermal growth factor; FGF, fibroblast growth factor; MCS, multicellular spheroids; CD133, cluster of differentiation 133; shRNA, short hairpin RNA; siRNA, small interfering RNA; AIF, apoptosis-inducing factor; ROS, reactive oxygen species; RNS, reactive nitrogen species; carboxy-PTIO, 2-(4-carboxyphenyl)-4,4,5,5-tetramethylimidazole-1-oxyl-3-oxide; RIP-1, receptor-interacting protein 1; zVAD, z-Val-Ala-DL-Asp(OMe)-fluoromethylketone; TRAIL, TNF-related apoptosis-inducing ligand; TNF, tumor necrosis factor; NOD/SCID gamma-chain deficient, non-obese diabetic/severe combined immunodeficiency gamma-chain deficient; TUNEL, terminal deoxynucleotidyl transferase dUTP nick-end labeling; PARP, poly-ADP-ribose-polymerase; FACS, fluorescence-activated cell sorting; EGFR, EGF receptor; Bak, Bcl-2 homologous antagonist/killer; PE, phycoerythrin; DMEM, Dulbecco's modified Eagle's medium; PBS, phosphate-buffered saline; TBST, tris-buffered saline tween 20; HRP, horseradish peroxidase; M-MLV, Moloney murine leukemia virus; cDNA, complementary DNA; 7-AAD, 7-aminoactinomycin D; BSA, bovine serum albumin; DAPI, 4',6-diamidino-2-phenylindole; OCT, optimal cutting temperature compound; PEG, polyethylene glycol; D5W, 5% dextrose in water; ANOVA, analysis of variance; LCNEC, large-cell neuroendocrine carcinoma; SCC, squamous cell carcinoma; AC, adenocarcinoma; DIC, differential interference contrast; WT, wild type; Mut, mutated; Stem, LCSC lines; Diff, differentiated; CAT, catalase

Received 19.7.13; revised 16.6.14; accepted 17.6.14; Edited by D Green; published online 18.7.14

of Bcl-2 family members in regulating the stem cell compartment is less clear. By analyzing the expression and relative function of Bcl-2 and Bcl-X_L in LCSC, we identified a prevalent role of Bcl-X_L in LCSC survival. Differently from chemotherapy, ABT-737 showed a preferential cytotoxic activity towards quiescent/slowly proliferating LCSC *in vitro* indicating a potential use of this inhibitor to eradicate chemotherapy-resistant LCSC. *In vivo*, ABT-737 blocked the progression of LCSC-derived xenografts and reduced CSC content, substantiating its specific effect on the CSC compartment. Altogether, these results indicate for the first time a key role of Bcl-X_L in LCSC, opening new perspectives for the elimination of therapy-resistant cells.

Results

Phenotypic and functional characterization of LCSCs.

Four LCSC lines were isolated from NSCLC surgical specimens (one large-cell neuroendocrine carcinoma, one adenocarcinoma and two squamous cell carcinomas; clinical and mutational data are reported in Supplementary Figure 1) and cultured in serum-free medium containing EGF and basic-FGF as previously described.⁴ Such culture conditions allow the growth of multicellular spheroids (MCSs) with properties of CSC, as demonstrated by their ability to generate tumors that phenocopy the original patient tumor in immunocompromised mice (Figure 1a). LCSC can be induced to differentiate by growth in adherent conditions (described in Materials and Methods), where they acquire the expression of cytokeratins and lose the expression of stem cell markers such as Nanog (Figure 1b). LCSC MCS express stem cell markers such as CD133, ALDH1 (detected as ALDH activity) and c-kit (Figures 1c–e). Notably, none of the three markers showed a high and consistent expression in all the LCSC lines, indicating a phenotypic heterogeneity in NSCLC stem cell marker expression as also reported by recent studies.¹⁵ Drug resistance has been previously demonstrated to be a feature of LCSC.^{4,6,16} As expected, LCSCs used for this study were highly resistant to commonly used antineoplastic agents (Figure 1f), whereas their differentiated progeny and the commercial cell line H460 were overall more sensitive to drug-induced death. Altogether, these observations substantiate the validity of LCSC as cellular models in the search of new options for lung cancer therapy.

Expression and RNA-mediated silencing of Bcl-2 family members in LCSCs.

Anti-apoptotic Bcl-2 family proteins have a key role in cancer cell survival and have been recently shown to contribute specifically to the maintenance of the CSC population in hematological malignancies.^{13,14} In order to evaluate the possible contribution of Bcl-2 family proteins in LCSC, we assessed the expression of Bcl-2, Bcl-X_L, Mcl-1, Bim, Puma and Noxa in LCSC and in their differentiated progeny by immunoblotting and flow cytometry analysis (Figure 2a and Supplementary Figure 2a, respectively). Bcl-X_L and Mcl-1 were ubiquitously expressed in LCSC and differentiated cells, whereas Bcl-2 was completely absent from two of the four LCSC lines examined, as confirmed also by analysis of LCSC RNA levels (Figure 2b). Pro-apoptotic

Bim, Puma and Noxa were variably expressed, with an overall tendency to increase with differentiation (Figure 2a), in line with the higher sensitivity of differentiated cells to cytotoxic drugs. To address the relative importance of Bcl-2, Bcl-X_L and Mcl-1 in LCSC survival, we silenced the expression of either factor with short duplexed RNA oligonucleotides in LCSC line LC1 (which expresses both Bcl-2 and Bcl-X_L) and in LC4 (which does not express Bcl-2). In addition, we double-silenced Bcl-2/Bcl-X_L in LC1. Western blot analysis of shRNA-treated LCSC showed that each siRNA pool had a prevalent effect in silencing its specific target (Figure 2c and Supplementary Figure 2c). Then, we assessed the functional outcome of Bcl-2, Bcl-X_L and Mcl-1 targeting in LCSC through analysis of cell viability, caspase 3/7 activation and clonogenicity. Bcl-2 silencing resulted in a moderate (~25%) decrease in LCSC viability, no apparent caspase 3/7 activation and modest inhibition of colony number/size in semisolid culture (Figures 2d–g). Differently, Bcl-X_L silencing resulted in a marked (~75%) reduction in cell viability and colony-forming capacity accompanied by significant caspase 3/7 activation. Mcl-1 silencing also resulted in strong (~75%) inhibition of LCSC viability and colony formation (Figures 2d–g). Combined silencing of both Bcl-2/Bcl-X_L in LC1 resulted in slightly higher inhibition of cell viability as compared with single Bcl-X_L silencing (~80%) and an increased effect on caspase activation and colony formation, with the complete disappearance of large colonies (Figures 2d–g). Single Bcl-X_L silencing in LC4 resulted in strong (~75%) inhibition of cell viability and colony formation (Figures 2d–g). These results indicate a major role for Bcl-X_L and Mcl-1 in LCSC survival and a further increased importance of Bcl-X_L in LCSC devoid of Bcl-2.

The small-molecule BH3 mimetic ABT-737 inhibits survival and self-renewal of LCSC *in vitro*.

Given the high *in vitro* efficacy of combined Bcl-2/Bcl-X_L silencing, we evaluated the effects of the Bcl-2/Bcl-X_L inhibitor ABT-737 on the survival of LCSC and of their differentiated counterparts. ABT-737 induced a significant reduction of viability in all LCSC lines starting from a 500-nM concentration (Figure 3a). ABT-737 toxicity was generally lower in differentiated cells, which in two out of four cases were sensitive only to the 1- μ M concentration (Figure 3a). In order to evaluate the relative contribution of Bcl-2 and Bcl-X_L inhibition in ABT-737-mediated toxicity, we treated LCSC and differentiated cells with the Bcl-2-selective inhibitor ABT-199. Such treatment resulted only in a modest decrease in cell viability in one out of four lines (Figure 3b). Likewise, ABT-737, but not ABT-199, significantly reduced colony number and size in all the LCSC lines (Figures 3c and d). These results indicate that the effects of ABT-737 in LCSC are mainly mediated through Bcl-X_L inhibition, whereas single Bcl-2 inhibition had negligible effects on cell survival. Propidium iodide staining and flow cytometry analysis of cellular DNA in ABT-737-treated LCSC showed that the decrease in cell number was actually because of an accumulation of cells with fragmented DNA, suggesting the occurrence of apoptosis.

ABT-737 preferentially eliminates quiescent/slow-proliferating LCSC. Quiescent/slow-proliferating CSCs have

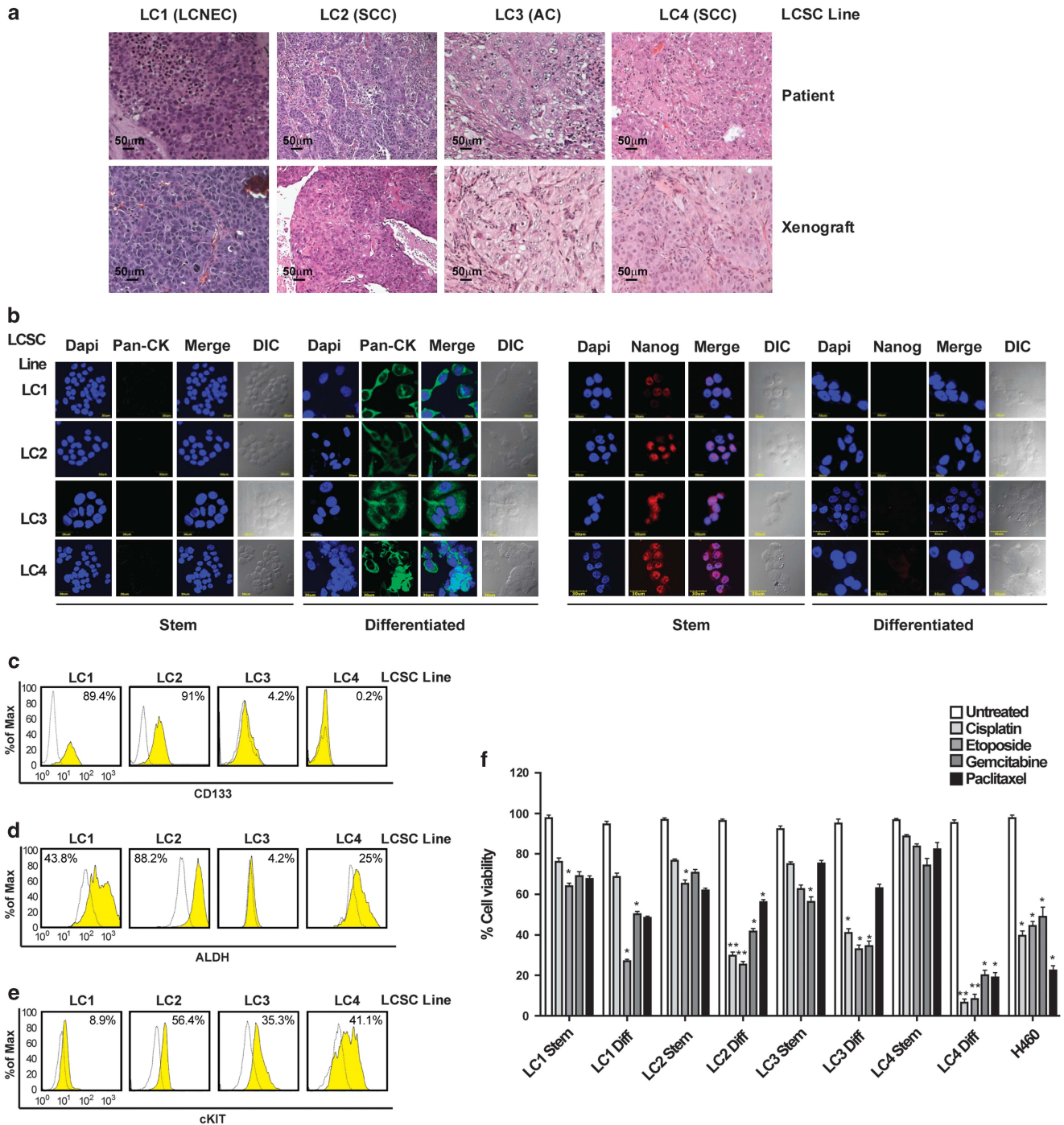


Figure 1 Phenotypic and functional characterization of LCSCs. (a) Hematoxylin–eosin-stained sections of patient tumors (upper panels) and of mouse xenografts (lower panels) obtained with the indicated LCSC lines. Magnification $\times 10$, bar $50 \mu\text{m}$. LCNEC, large cell neuroendocrine carcinoma; SCC, squamous cell carcinoma; AC, adenocarcinoma. (b) Immunofluorescence analysis of cytokeratins and Nanog expression in LCSC grown as tumor spheroids (Stem) or in adherent conditions (Differentiated). DIC, differential interference contrast. Magnification $\times 60$, $\times 2$ zoom, bar $30 \mu\text{m}$. (c–e) Expression of CD133, ALDH-1 (measured indirectly as ALDEFLUOR positivity) and c-kit (cKIT) detected by flow cytometry in the indicated LCSC lines. (f) Viability of LCSC lines (Stem) and of their differentiated counterparts (Diff) treated for 72 h with gemcitabine $250 \mu\text{M}$, paclitaxel 30 ng/ml , cisplatin $5 \mu\text{g/ml}$ or etoposide $10 \mu\text{g/ml}$. Bars represent mean \pm S.D.; * $P \leq 0.05$ and ** $P \leq 0.01$ ($n = 3$). The NSCLC cell line H460 was used as a control

been identified in several tumors^{17–21} and in several cases have been specifically shown to represent the chemotherapy-resistant population (reviewed in Moore and Lyle²²). In order to determine whether LCSC populations separated according

to proliferation rates were differently affected by ABT-737 treatment, we stained LCSC with PKH26. This lipophilic dye is segregated between daughter cells with each round of division and therefore, after several days, is retained at high levels only

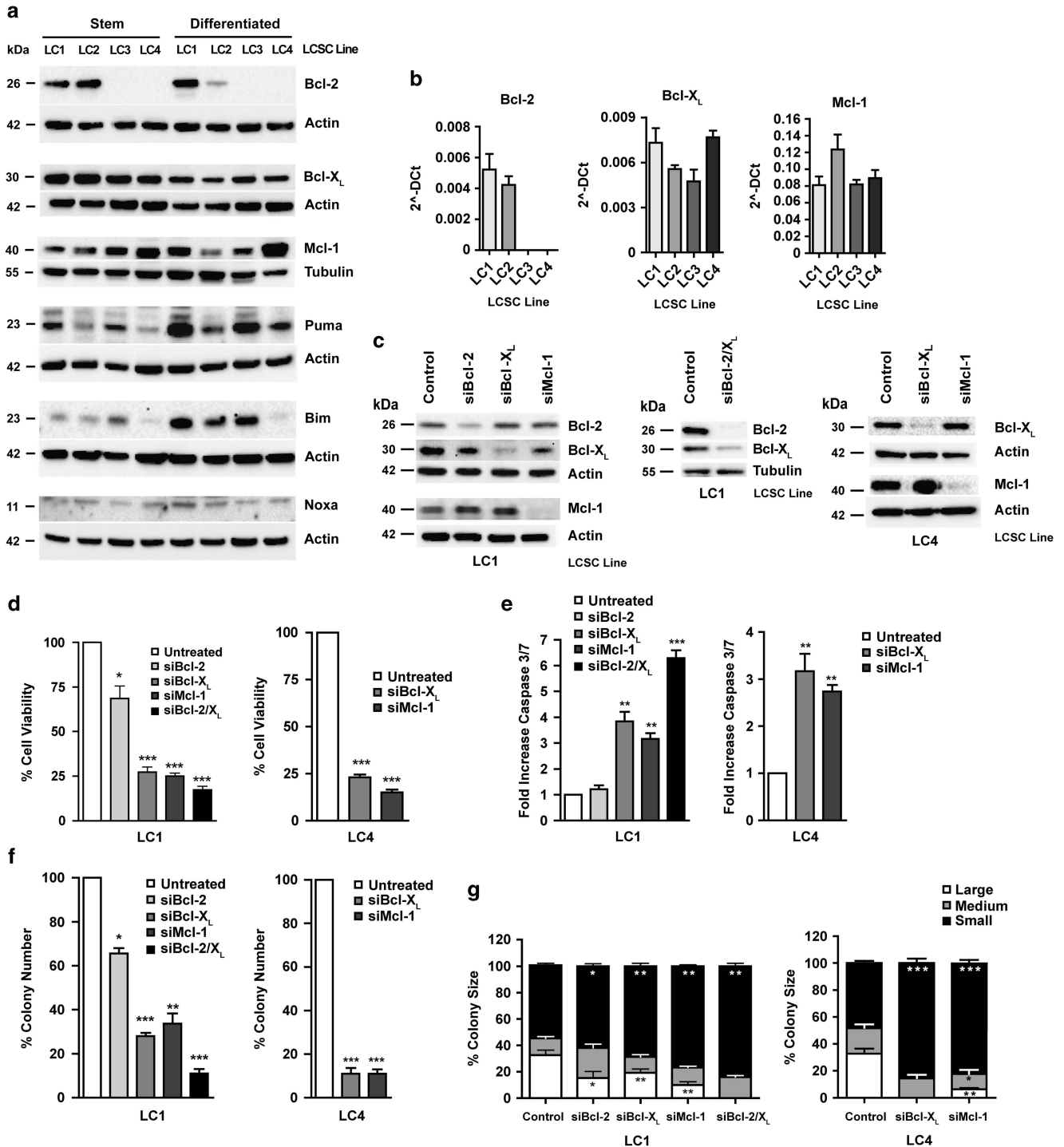


Figure 2 Expression of Bcl-2 family members in stem/differentiated lung cancer cells and functional effects of RNA-mediated silencing. (a) Western blot analysis of Bcl-2, Bcl-X_L, Bim, Puma, Noxa and Mcl-1 expression in LCSC (Stem) and their differentiated progeny (Differentiated). (b) Real-time PCR analysis of Bcl-2, Bcl-X_L and Mcl-1 transcripts in LCSC. (c) Western blot analysis of Bcl-2, Bcl-X_L and Mcl-1 expression in LCSC LC1 (left and center) and LC4 (right) transfected with short-hairpin RNAs non-targeting (Control) or directed against Bcl-2 (siBcl-2), Bcl-X_L (siBcl-X_L), combined (siBcl-2/X_L) or Mcl-1 (siMcl-1). (d) Viability of LCSC LC1 and LC4 transfected as above. Bars represent mean \pm S.D.; * $P \leq 0.05$ and *** $P \leq 0.001$ ($n = 3$). (e) Caspase 3/7 activation, expressed as an increase compared with controls, of LCSC LC1 and LC4 transfected as above. Bars represent mean \pm S.D.; ** $P \leq 0.01$ and *** $P \leq 0.001$ ($n = 3$). (f) Colony formation in soft-agar culture of LCSC LC1 and LC4 transfected as above (left). Bars represent mean \pm S.D.; * $P \leq 0.05$, ** $P \leq 0.01$ and *** $P \leq 0.001$ ($n = 3$). (g) Size of colonies formed in soft-agar by LCSC LC1 (left) and LC4 (right) transfected as above. Asterisks refer to the statistical significance of the number of small (black bands), medium (grey bands) and large (white bands) colonies compared between each sample and the control. Bars represent mean \pm S.D.; * $P \leq 0.05$, ** $P \leq 0.01$ and *** $P \leq 0.001$ ($n = 3$)

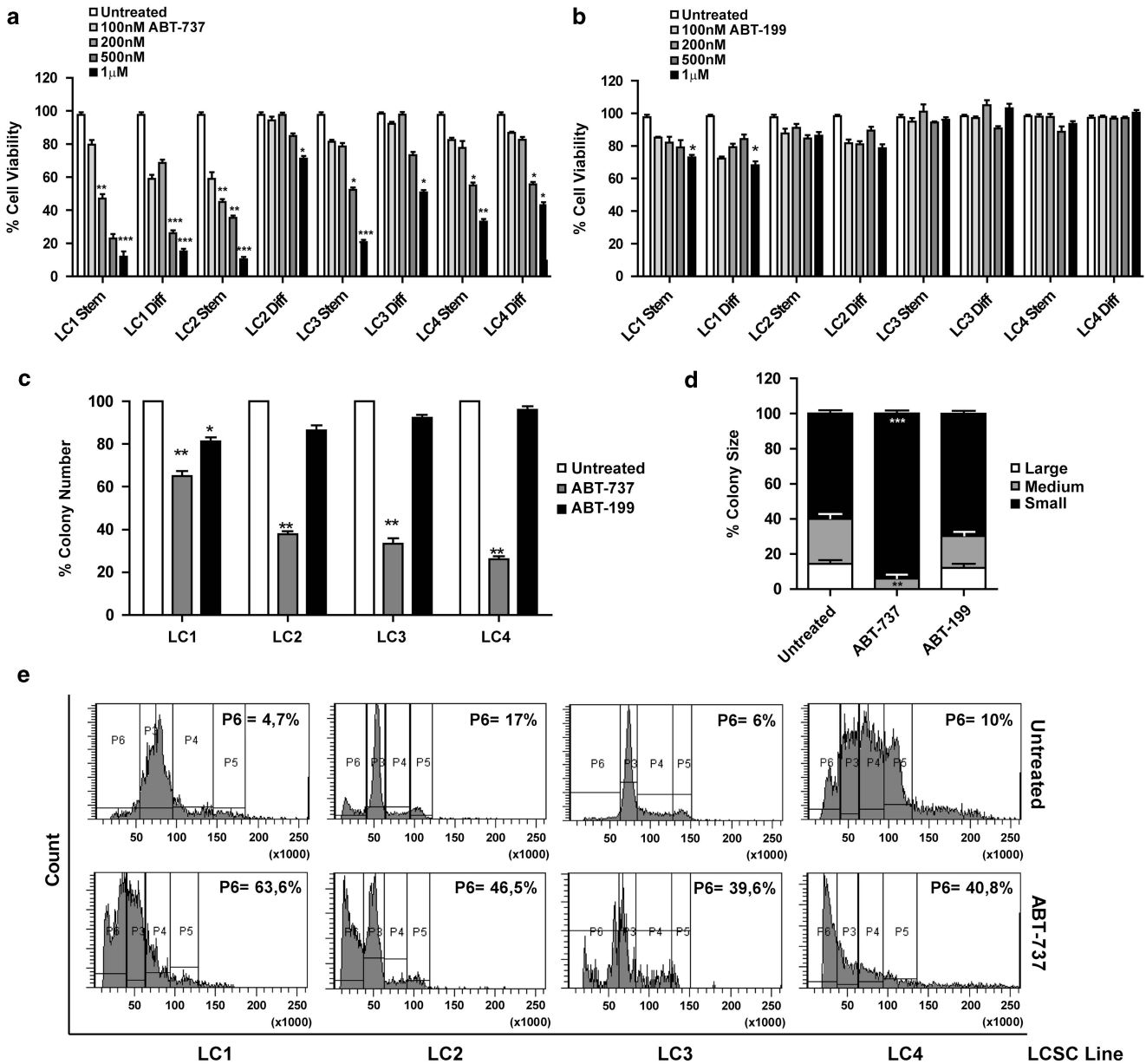


Figure 3 Effect of ABT-737 on LCSC *in vitro*. (a) Viability of LCSC (Stem) and their differentiated counterparts (Diff) treated with increasing doses of ABT-737 (100 nM–1 μ M) for 72 h. Bars represent mean \pm S.D.; * $P \leq 0.05$, ** $P \leq 0.01$ and *** $P \leq 0.001$ ($n = 5$). (b) Viability of LCSC treated with increasing doses of ABT-199 (100 nM–1 μ M) for 72 h. Bars represent mean \pm S.D.; * $P \leq 0.05$ ($n = 3$). (c) Colony formation in soft-agar culture of LCSC plated in the presence of 500 nM ABT-737 (ABT-737) or 500 nM ABT-199 (ABT-199). Bars represent mean \pm S.D.; * $P \leq 0.05$ and ** $P \leq 0.01$ ($n = 3$). (d) Size of colonies formed in soft-agar assay by LCSC LC1 treated as in c. Bars represent mean \pm S.D.; ** $P \leq 0.01$ and *** $P \leq 0.001$ ($n = 3$). Asterisks refer to the statistical significance of the number of small (black bands), medium (grey bands) and large (white bands) colonies compared between each sample and the control. (e) Propidium iodide staining and flow cytometry analysis of LCSC untreated (upper panels) or treated for 72 h with 500 nM ABT-737 (lower panels). Numbers refer to the percentage of events included in the P6 (hypodiploid) area of the plot

by slow-proliferating cells (Figure 4a). Ten days after PKH staining, LCSCs were sorted into PKH_{low} and PKH_{high} populations according to dye retention (Figure 4b), treated with ABT-737 or gemcitabine and cell viability was evaluated after 72 h as compared with mock-sorted cells. Quiescent/slow-proliferating PKH_{high} LCSCs were significantly more sensitive to ABT-737 than rapidly proliferating PKH_{low} cells, indicating that quiescent LCSCs have an increased dependence on Bcl-2 family proteins for survival (Figure 4c). By contrast, gemcitabine was more effective on rapidly

proliferating PKH_{low} cells, in line with the inability of chemotherapy to eradicate a fraction of therapy-resistant LCSC. Then, we analyzed the levels of pro- and anti-apoptotic Bcl-2 family members in PKH_{low} and PKH_{high} cells using flow cytometry in two LCSC lines (Figure 4d and Supplementary Figure 3) and we found that Bcl-X_L was consistently expressed at higher levels in PKH_{high} cells, according to their increased sensitivity to ABT-737. Bcl-2 was also expressed at higher levels in PKH_{high} LC1. In addition, we found that Noxa was significantly more expressed by quiescent PKH_{high} cells

as compared with PKH_{low} cells in the two LCSC lines examined, although the significance of this finding is unclear. The other Bcl-2 family members Mcl-1, Bim and Puma showed a trend towards a higher expression in PKH_{high} cells but the overall difference between PKH_{low} and PKH_{high} cells was not significant. Altogether, these results substantiate a role of Bcl-X_L in the survival of quiescent LCSC and support further investigations on targeted therapeutic strategies.

Functional characterization of ABT-737-induced death in LCSC. To gain insights into the mechanisms of ABT-737-induced death in LCSC, we first examined the involvement of mitochondria, which represent the preferential cellular location of Bcl-2 and Bcl-X_L and the hub of apoptosis-related events.²³ First, we evaluated mitochondrial membrane

potential through JC-1 staining of live LCSC MCS. Whereas untreated MCS showed red JC-1 aggregates typical of healthy mitochondria, a significant proportion of ABT-737-treated MCS displayed only green JC-1 monomers, indicating the occurrence of mitochondrial depolarization (Figure 5a). Immunofluorescence staining of dissociated LCSC showed redistribution of cytochrome *c* and apoptosis-inducing factor (AIF) from mitochondria to the nucleus and cytoplasm of ABT-737-treated cells (Figures 5b and c). Mitochondrial depolarization, together with cytochrome *c* and AIF release, indicate that ABT-737-induced death has some features of apoptosis. Modest (three- to sixfold increase) caspase 3/7 activation was detectable in 2/4 LCSC lines treated with ABT-737, reaching maximal levels after 16 h of stimulation (Figures 5d and e). As overproduction of reactive oxygen

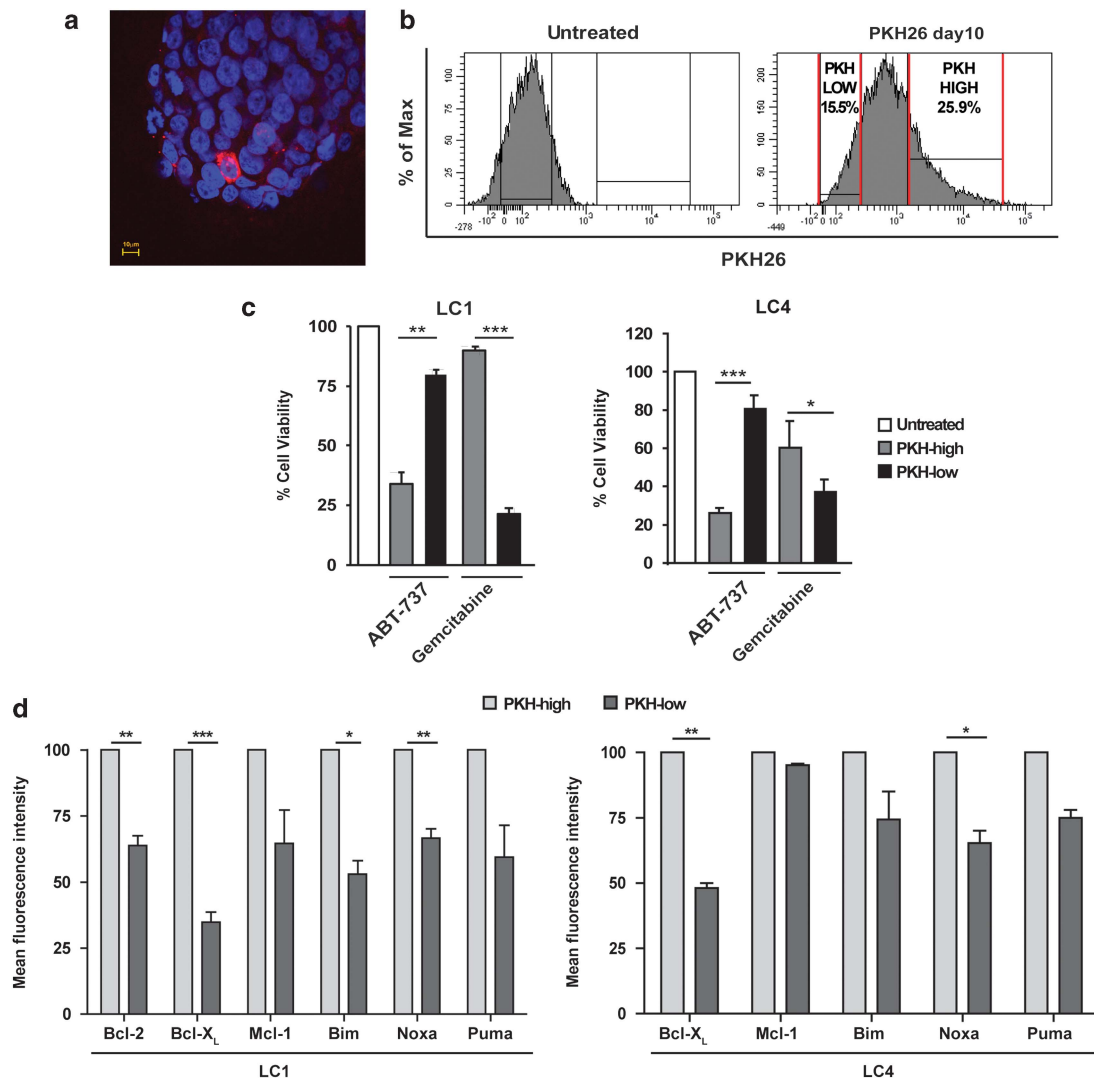


Figure 4 ABT-737 preferentially eliminates quiescent/slow cycling LCSC. (a) Representative confocal image of a LCSC spheroid (line LC4) 10 days after PKH26 staining. Red: PKH26, blue: Dapi. Magnification $\times 60$, bar $10 \mu\text{m}$. (b) Representative FACS profile of LCSC cell populations (line LC4) selected for sorting 10 days after PKH26 staining (PKH26 day 10) as compared with the unstained control (Untreated). (c) LCSC lines LC1 and LC4 mock-sorted (Untreated) or sorted into PKH26 high and PKH26 low populations were incubated for 72 h with 500 nM ABT-737 or 250 μM gemcitabine and cell viability was assessed as described in Materials and Methods. Bars represent mean \pm S.D.; * $P \leq 0.05$, ** $P \leq 0.01$ and *** $P \leq 0.001$ ($n = 3$). (d) Levels of Bcl-2 family members in PKH26 high (PKH high) and PKH26 low (PKH low) LCSC populations (lines LC1 and LC4) measured by flow cytometry and expressed as normalized mean fluorescence intensity. Bars represent the mean \pm S.D.; * $P \leq 0.05$, ** $P \leq 0.01$ and *** $P \leq 0.001$ ($n = 4$). Raw data of one representative experiment are shown in Supplementary Figure 3

species (ROS) and reactive nitrogen species (RNS) has been implicated in cell death induction, we determined whether oxidative/nitrosative stress was implicated in ABT-737-induced death in LCSC. To do this, we treated cells with ABT-737 in the presence of radical scavengers such as superoxide dismutase, catalase (ROS scavengers), carboxy-PTIO and uric acid (blockers of nitrogen radicals). Surprisingly, neither of these compounds was able to significantly reduce ABT-737-induced death (Figure 5f), suggesting that ROS/RNS are dispensable for ABT-737-induced LCSC death. Finally, we determined whether ABT-737-induced death could be affected by caspase inhibition or RIP-1 inhibition, thus indicating prevalent features of caspase-mediated apoptosis or necroptosis, respectively. LCSCs were treated for 48 h with ABT-737 in the presence of the pan-caspase inhibitor zVAD, of the RIP-1 inhibitor necrostatin or with a combination of the two (Figure 5g). To assess the possible baseline toxicity of the inhibitors, LCSCs were also treated with the single drugs or with their combination in the absence of ABT-737. Controls of inhibitor efficacy were represented by Jurkat leukemia cells treated with TRAIL and by L929 mouse fibrosarcoma cells treated with TNF (Supplementary Figure 4). zVAD and necrostatin as single agents were unable to inhibit ABT-737-induced LCSC death, which was even slightly enhanced in the presence of the inhibitors. The simultaneous presence of the two inhibitors was similarly unable to block ABT-737-induced death, indicating that it occurs through mechanisms alternative to caspase-dependent apoptosis or necroptosis.

ABT-737 blocks the growth of CSC-derived tumor xenografts and reduces stem cell content *in vivo*. To determine the *in vivo* antitumor efficacy of ABT-737, we generated subcutaneous tumor xenografts by injecting LCSC into immunocompromised (NOD/SCID gamma-chain-deficient) mice. When tumors reached the approximate volume of 200–250 mm³, mice were treated for 3 weeks with either vehicle alone, gemcitabine or ABT-737. Experiments were performed both with LC1 (Figure 6a) and LC4 (Figure 6b) LCSC lines, as representatives of cells expressing both Bcl-2/Bcl-X_L or only Bcl-X_L, respectively. In both cases, ABT-737 treatment abrogated tumor growth, whereas gemcitabine treatment had only a moderate inhibitory effect (Figures 6a and b). Hematoxylin–eosin evaluation of tissue structure showed the presence of necrotic areas and decreased cellularity in ABT-737-treated samples as compared with control or gemcitabine-treated samples (Figure 6c). To gain more insights into the ability of ABT-737 to target LCSC *in vivo*, we performed double stainings for CD133 and either terminal deoxynucleotidyl transferase-mediated dUTP nick end labeling (TUNEL; to detect the occurrence of DNA fragmentation), poly-ADP-ribose-polymerase (PARP) cleavage or caspase-3 activation in tumor xenografts of the LCSC line LC1 treated with ABT-737. Positivity for CD133 was often associated with TUNEL staining, cleaved PARP and active caspase-3 in ABT-737-treated samples but not in chemotherapy-treated samples, indicating that ABT-737 treatment induces LCSC death *in vivo* (Supplementary Figure 5). This hypothesis was substantiated by the evaluation of residual LCSC numbers at the end of treatment,

which was measured with FACS analysis of ALDH activity (ALDEFLUOR) in dissociated xenograft cells. We found a significantly reduced content of ALDEFLUOR-positive cells in ABT-737-treated xenografts as compared with control xenografts derived from LC1 and LC4 (Figures 6d and e). By contrast, gemcitabine treatment resulted in a significant increase in ALDEFLUOR-positive cells in LC1 and in LC4, suggesting that gemcitabine antineoplastic activity is due mainly to an effect on non-stem tumor cells.

Discussion

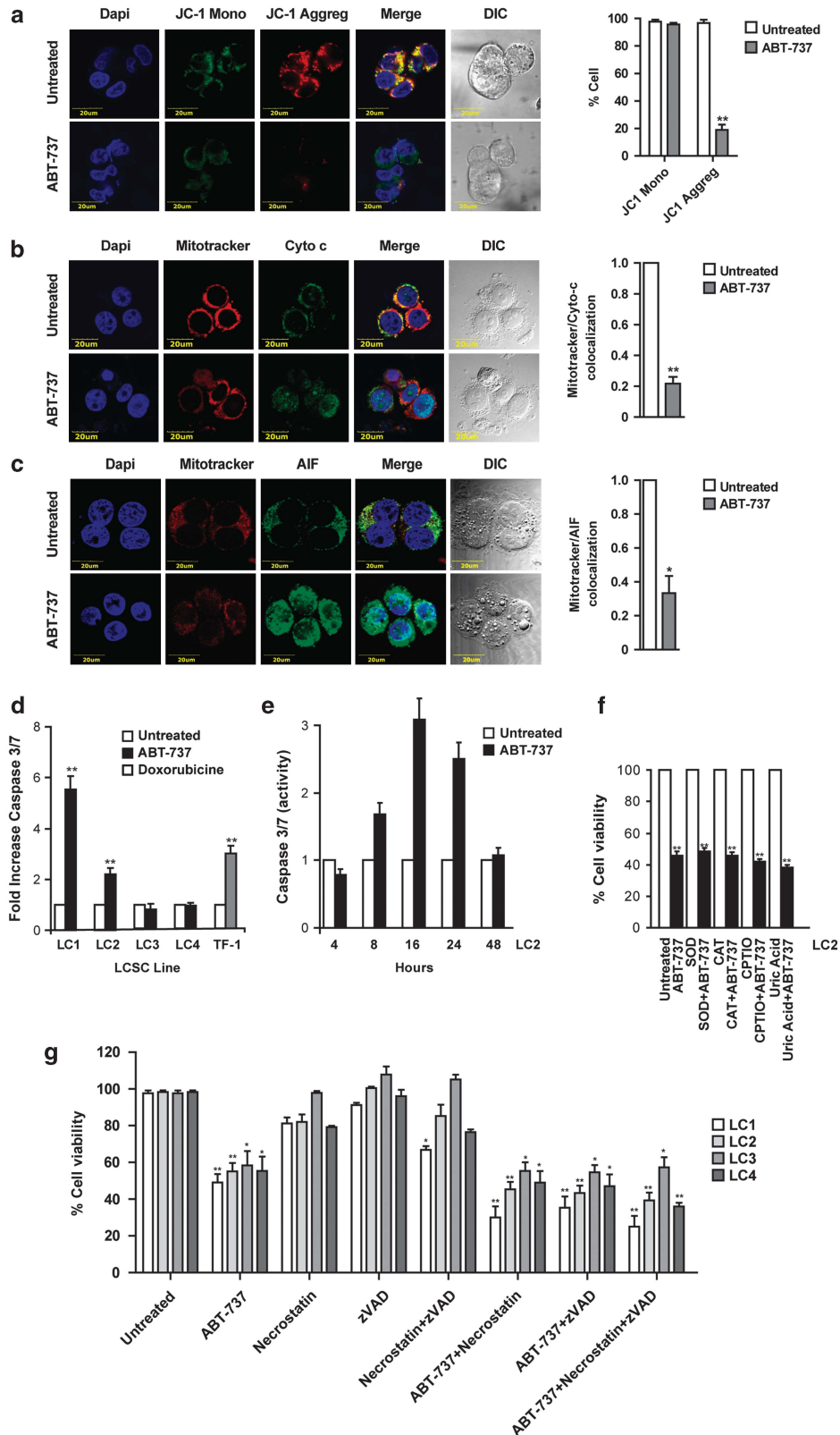
The advent of molecularly targeted therapies has increased survival in a subset of lung cancer patients but did not radically change disease outcome because of the invariable occurrence of therapy resistance and tumor relapse. CSCs have been indicated as the population responsible for therapy resistance, because of their increased availability of drug-protective mechanisms.²⁴ Quiescence is a common feature of drug-resistant cells and has been associated with stem cell traits in several tumors.²² In glioblastoma, quiescent CSCs have been demonstrated to selectively resist temozolomide treatment and to regenerate the tumor after chemotherapy.²⁵ Interestingly, quiescent CSC populations in leukemias have been recently shown to express high levels of Bcl-2 and to rely on this factor for oxidative phosphorylation, which represents their main energy-generating pathway. In AML and CML, Bcl-2 inhibition by ABT-737 selectively targets quiescent CSC, representing a proof-of-principle for investigating a similar approach in solid tumors.^{13,14} NSCLC commercial cell lines have been reported to be moderately sensitive to ABT-737 as a single agent.^{26,27} However, lung tumor cells that survive treatment with EGFR kinase inhibitors show decreased proliferation and increased sensitivity to ABT-737,²⁸ suggesting the existence of a link between quiescence, Bcl-2 family members and drug resistance in lung cancer cells.

In patient-derived LCSC spheroids we found a constant expression of Bcl-X_L, but not Bcl-2, confirming the observations reported by Fan *et al.*²⁸ in lung cancer cell lines. Importantly, Bcl-X_L inhibition was more effective than Bcl-2 inhibition in decreasing LCSC viability and clonogenic capacity in LCSC lines expressing both factors. This observation is consistent with the fact that Bcl-X_L binds a larger number of pro-apoptotic partners than Bcl-2 and seems to have a major role in the control of drug-induced apoptosis,²⁹ thus emerging as a promising therapeutic target. However, future targeted therapies specifically directed against Bcl-X_L would have to face the problem of therapy-induced thrombocytopenia, as Bcl-X_L has been shown to be essential for platelet survival.³⁰ One way to overcome this obstacle may be the design of novel Bcl-X_L inhibitors with selective toxicity against tumor cells but not against platelets, based on the difference between the survival complexes active in the two cellular systems (Bcl-X_L/Bim in tumor cells and Bcl-X_L/Bak in platelets).²⁹

ABT-737 induced in LCSC a form of cell death that was insensitive to inhibition of caspases, of ROS/RNS and of necroptosis. The occurrence of mitochondrial depolarization and cytochrome *c* release suggests that ABT-737 may induce in LCSC a non-canonical form of apoptotic cell death that can

include caspase activation as a non-essential pathway. Notably, ABT-737-induced death has been shown to be ROS-dependent in other cellular systems.^{31,32} This difference

may be ascribed to the peculiar oxidative state of CSCs, which have been reported to have low levels of ROS and increased expression of free radical-scavenging systems.^{9,33}



The ability of ABT-737 to target LCSC was confirmed *in vivo*, where ABT-737 treatment arrested the growth of LCSC-derived tumors and significantly reduced the amount of stem cells present in the xenograft. This finding has important implications for the therapy of NSCLC, suggesting that treatment with ABT-737 could effectively complement a first line of therapy with chemotherapy or tyrosine kinase inhibitors in order to target residual quiescent LCSC. Owing to its ability to preferentially kill quiescent LCSC, ABT-737 treatment may not result in a fast macroscopic reduction of tumor size but may have long-term beneficial effects on the rates of tumor growth and relapse. Clinical trials designed to specifically evaluate this endpoint will help to clarify the usefulness of Bcl-X_L inhibition in the treatment of NSCLC patients.

Materials and Methods

Antibodies and reagents. ABT-737 was provided by AbbVie (Abbott Park, IL, USA). ABT-199 was purchased from Selleckchem (Munich, Germany). CD133/1-PE (used for flow cytometry) and CD133/2 (used for immunofluorescence) were from Miltenyi Biotec (Bergisch Gladbach, Germany). ALDEFLUOR assay was from Aldagene (Durham, NC, USA). Nanog and AIF antibodies were from Cell Signaling Technology Inc. (Danvers, MA, USA). Pan-cytokeratin antibody was from Dako (Glostrup, Denmark). Cytochrome *c* antibody was from BD Biosciences (San José, CA, USA). Cleaved caspase 3 antibody was from Upstate Biotechnology (Lake Placid, NY, USA). Alexa Fluor-conjugated secondary antibodies were from Invitrogen-Molecular Probes (Eugene, OR, USA). TUNEL was from Roche Molecular Biochemicals (Indianapolis, IN, USA). Bcl-X_L (clone H5), Bcl-2 (clone DC-21), Mcl-1 (clone C-2), Bim (clone H-5), Puma (clone H-136), Noxa (clone FL-54) and necrostatin were from Santa Cruz Biotechnology (Santa Cruz, CA, USA). Monoclonal antibodies anti-actin, tubulin and cleaved PARP were from Sigma Aldrich (St Louis, MO, USA). Secondary anti-mouse and anti-rabbit antibodies coupled to horseradish peroxidase were from GE Healthcare (Uppsala, Sweden).

CSC isolation and culture. LCSCs were isolated as previously described from surgically resected tumor samples through selective culture in serum-free medium containing EGF 20 ng/ml and basic FGF 10 ng/ml (PeproTech, London, UK).⁴ Nontreated polystyrene flasks (Thermo Fischer Scientific, Waltham, MA, USA) were used to reduce cell adherence and support growth of LCSC as multicellular spheres. Regular thawing of early-passage cells was carried out to avoid the accumulation of culture-related changes. LCSC differentiation was obtained by culture for 24 h in DMEM 10% plus fetal bovine serum (Gibco-Invitrogen, Carlsbad, CA, USA) and for 5 additional days in Bronchial Epithelial Cell Growth Medium (Cambrex, East Rutherford, NJ, USA).

Viability assay. LCSC viability upon treatment with chemotherapeutic drugs, ABT-737 and other inhibitors was determined with the CellTiter-Glo assay (Promega, Madison, WI, USA) according to the manufacturer's instructions. Briefly, 1.5×10^3 dissociated LCSC, H460, Jurkat or TF-1 cells were plated in 96-well flat bottom plates. Chemotherapeutic agents were added at the following final concentrations: gemcitabine 250 μ M, paclitaxel 30 ng/ml, cisplatin 5 μ M/ml

and etoposide 10 μ M/ml. Pan-caspase inhibitor z-Val-Ala-Asp-fluoromethylketone (40 μ M; Bachem, Bubendorf, Switzerland) or 25 μ M necrostatin (Santa Cruz Biotechnology) were added 1 h before ABT-737 and cells were processed after 3 additional days. TNF- α was kindly provided by Dr. TL Haas (see Acknowledgements and studies by Haas *et al.*,³⁴ Enyedy *et al.*³⁵ and Ewald *et al.*³⁶). Free radical scavengers used to inhibit ROS (superoxide dismutase and catalase 1 μ M/ml each), nitric oxide (carboxy-PTIO 0.1 μ M) and peroxynitrite (uric acid 1 μ M) were added 24 h before ABT-737 and cell viability was determined after 3 additional days of incubation.

RNA interference. In all, 1.25×10^5 LCSCs were plated on six-well plates in antibiotic-free culture medium and incubated for 4 h at 37 °C in the presence of 320 nM ON-TARGETplus SMARTpool siRNA (D-001810-01-055 Non-targeting siRNA, L-003307-00-0005 Human Bcl-2 and L-003458-00-0005 Human Bcl-X_L, M-004501-08-0005 Human Mcl-1 Dharmacon/Thermo Scientific, Lafayette, CO, USA) and 5 μ l Lipofectamine 2000 (Invitrogen). After 4 h the transfection mixture was substituted with LCSC culture medium and cells were analyzed for protein expression, viability and caspase activation at the indicated times.

PKH26 staining. LCSC spheroids were dissociated with TrypLE Express (Invitrogen) and stained for 1 h at 37 °C with 1 : 500 PKH26 (Sigma-Aldrich), then washed extensively with PBS and cultured for 10 additional days. Cells were then separated with a FACS Aria (BD Biosciences) into PKH_{low} and PKH_{high} fractions. Control cells did not undergo PKH26 staining but were mock-sorted to induce similar stress conditions as in the other sorted samples.

Western blotting. LCSC spheroids were lysed in 1% NP40 lysis buffer (20 mM Tris HCl pH 7.2, 200 mM NaCl, 1% NP40) supplemented with protease inhibitor cocktail and phosphatase inhibitor cocktails I and II (all from Sigma-Aldrich). Lysate concentrations were determined by the Bradford assay (Bio-Rad Laboratories, Hercules, CA, USA). Proteins were loaded on a 4–12% precast gel (Invitrogen) and transferred to nitrocellulose membranes. Blots were blocked with TBST 5% nonfat dry milk and incubated overnight at 4 °C with primary antibodies, and then incubated for 45 min with secondary HRP-conjugated antibodies dissolved in TBST 1% BSA. Chemiluminescence was detected with Super SignalWest Pico (Thermo Fisher Scientific/Pierce, Waltham, MA, USA).

Clonogenicity assay. The clonogenic capacity of LCSC was assessed by plating 500 cells per well in triplicate in 24-well plates containing a soft agar bilayer (0.3% top and 0.4% bottom layer, SeaPlaque Agarose, Cambrex) with or without ABT-737 or ABT-199. Cultures were incubated at 37 °C for 21 days. Colonies were stained with crystal violet (0.01% in 10% methanol) and counted under a light microscope. Data shown represent the percentage of colonies normalized to the number of plated cells.

Cell cycle, apoptosis, necroptosis and caspase activation assays. Cell cycle analysis was performed by staining dissociated LCSC spheroids with 50 μ M propidium iodide dissolved in buffer 0.1% trisodium citrate, 9.65 mM NaCl, 0.1% NP40, 200 μ M/ml RNase for 1 h at room temperature. Samples were analyzed with a FACS Canto flow cytometer (BD Biosciences). Evaluation of caspase activity was determined with the Apo-ONE Homogeneous Caspase-3/7 Assay kit (Promega) at indicated times. Luminescent or fluorimetric assay signals were read using a DTX880 multimode microplate reader (Beckman Coulter, Brea, CA, USA). The occurrence of necroptosis was evaluated by treating

Figure 5 Characterization of ABT-737-induced death in LCSC. (a) Left: immunofluorescence staining of live intact spheroids, untreated or treated with 500 nM ABT-737 for 48 h with the mitochondrial membrane sensor JC-1, indicating the presence of depolarized mitochondria as loss of red JC-1 aggregates. Magnification $\times 60$, $\times 3.5$ zoom, bar 20 μ m. Right: quantification of JC1 monomers and aggregates in untreated and ABT-737-treated cells on confocal samples; $**P \leq 0.01$ ($n = 3$). (b) Left: cytochrome *c* localization in LCSC pre-stained with Mitotracker Red and untreated or treated with 500 nM ABT-737 for 48 h. Magnification $\times 60$, $\times 3$ zoom, bar 20 μ m. Right: quantification of Mitotracker/cytochrome *c* colocalization in confocal samples; $**P \leq 0.01$ ($n = 3$). (c) Left: localization of apoptosis inducing factor (AIF) in LCSC pre-stained with Mitotracker Red and untreated or treated with 500 nM ABT-737 for 48 h. Magnification $\times 60$, zoom $\times 3$, bar 20 μ m. Right: quantification of Mitotracker/AIF colocalization in confocal samples; $*P \leq 0.05$ ($n = 3$). The LCSC line LC1 was used to produce images shown in a–c. (d) Caspase 3/7 activation, expressed as fold increase as compared with untreated samples, in LCSC lines treated for 72 h with 500 nM ABT-737. The hematopoietic cell line TF-1 treated with 0.5 μ M doxorubicine was used as positive control. Bars represent mean \pm S.D.; $**P \leq 0.01$ ($n = 3$). (e) Time-course evaluation of caspase 3/7 activation in LC1 during the first 48 h of treatment with 500 nM ABT-737. (f) Viability of LCSC treated for 72 h with 500 nM ABT-737, alone (ABT-737) or in the presence or in the absence of free radical scavengers: SOD, superoxide dismutase; CAT, catalase; CPTIO, 2-(4-Carboxyphenyl)-4,4,5,5-tetramethylimidazole-1-oxyl-3-oxide. Bars represent mean \pm S.D.; $**P \leq 0.01$ ($n = 4$). (g) Viability of LCSC lines LC1-4 treated for 48 h with either 500 nM ABT-737, 40 μ M zVAD, 25 μ M necrostatin or the indicated combinations; $*P \leq 0.05$, $**P \leq 0.01$ ($n = 3$)

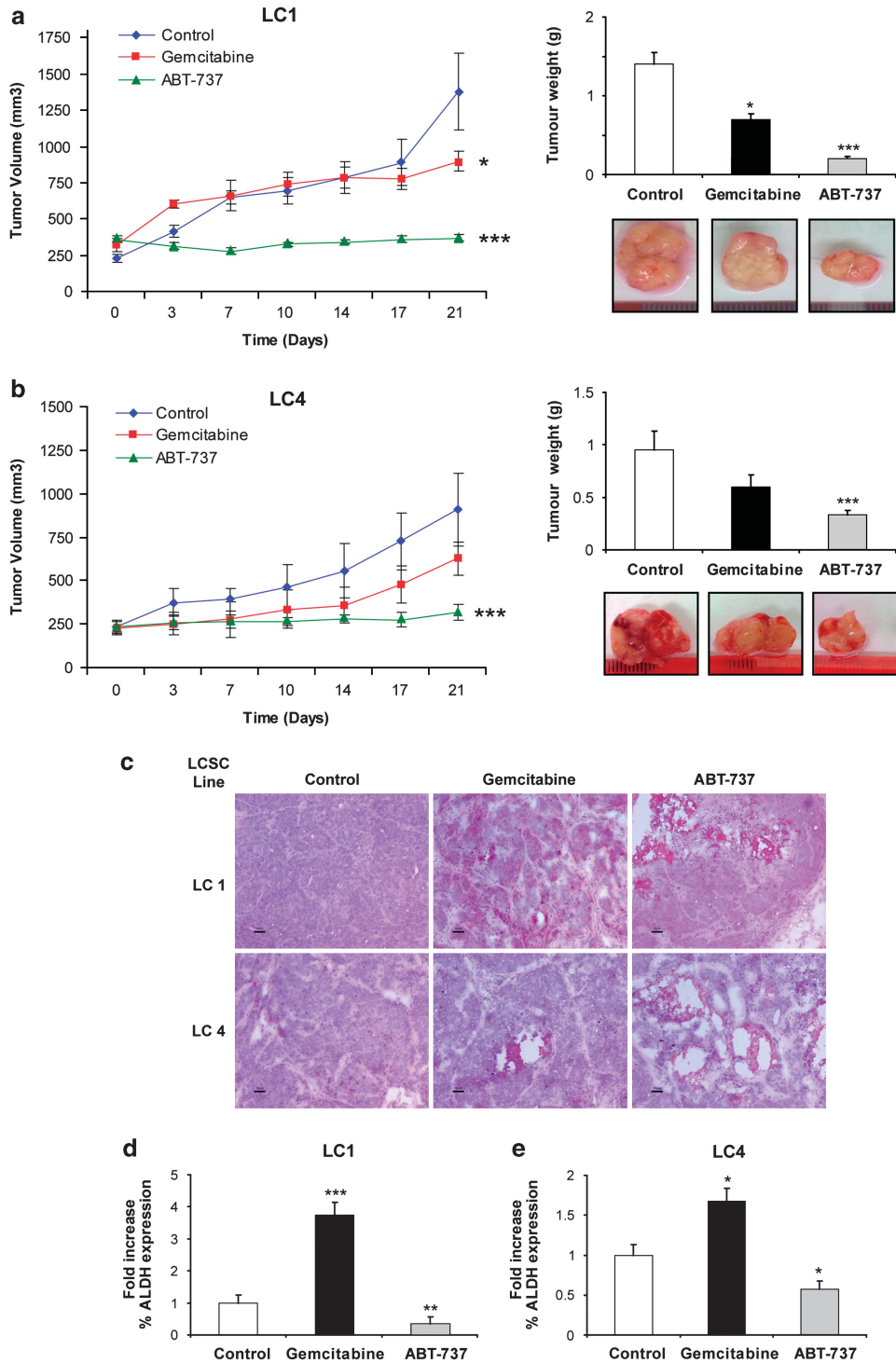


Figure 6 ABT-737 blocks the growth of LCSC-derived xenografts and reduces LCSC content *in vivo*. (a) Growth of tumor xenografts derived from the LCSC line LC1 in mice treated with vehicle (Control), gemcitabine or ABT-737 as described in Materials and Methods (left), tumor weight at the end of the experiment and representative picture of the tumors (right). Bars represent mean \pm S.D.; * $P \leq 0.05$ and *** $P \leq 0.001$ ($n = 3$). (b) Growth of tumor xenografts derived from the LCSC line LC4 and treated as above (left), tumor weight at the end of the experiment and representative picture of the tumors (right). Bars represent mean \pm S.D.; *** $P \leq 0.001$ ($n = 3$). (c) Hematoxylin–eosin-stained sections of xenografts derived from the LCSC lines LC1 and LC4 after 3 weeks of treatment with vehicle (Control), gemcitabine or ABT-737 as described above; $\times 10$ magnification, bar $50 \mu\text{m}$. (d) Fold variation of ALDEFLUOR-positive cells in gemcitabine- and ABT-737-treated tumor xenografts obtained with the LC1 LCSC line as compared with vehicle-treated controls. Bars represent mean \pm S.D.; ** $P \leq 0.01$ and *** $P \leq 0.001$ ($n = 3$). (e) Fold variation of ALDEFLUOR-positive cells in gemcitabine and ABT-737-treated tumor xenografts obtained with the LC4 LCSC line as compared with vehicle-treated controls. Bars represent mean \pm S.D.; * $P \leq 0.05$

LCSC with 500 ng/ml ABT-737 plus 25 μ M necrostatin for 48 h or L929 mouse fibrosarcoma cells with 100 ng/ml TNF plus zVAD 40 μ M plus 25 μ M necrostatin for 24 h.

Quantitative real-time PCR. Total RNA was extracted with TRIzol (Invitrogen). RNA (1 μ g) was reverse-transcribed with M-MLV reverse transcriptase (Gibco-Invitrogen) and cDNA was used as template in the subsequent PCR reactions. SYBR Green specific primers (Life Technologies, Carlsbad, CA, USA) were used for Bcl-2 (forward primer: 5'-CGGAGGCTGGGATGCCCTTTG-3'; reverse primer: 5'-GATGCAAGCTCCCACCAGGG-3'), Bcl-X_L (forward primer: 5'-GCCTAAGCGGATTGAATCTCT-3'; reverse primer: 5'-GCTCCCGGTTGC TCTGAGAC-3') and Mcl-1 (forward primer: 5'-AGGCTGGGATGGGTTTGTGG-3'; reverse primer: 5'-TGGCTAGGTTGCTAGGGTGC-3') quantitative PCR. Normalization was performed using GAPDH as reference (forward primer: 5'-GAGTCA ACGGATTTGGTCTGT-3'; reverse primer: 5'-TGGAAGATGGTATGGGATT-3'). Values are expressed in terms of $2^{-\Delta\Delta C_t}$ where $\Delta\Delta C_t = \Delta C_{t\text{sample}} - \Delta C_{t\text{calibrator}}$; ΔC_t is the difference in threshold cycles between the specific RNA and GAPDH amplicons, and C_t is a parameter given by the StepOne Plus Real-Time PCR software (Life Technologies) by negative correlation with an internal reference dye (ROX).

Flow cytometry. For flow cytometry assays, MCS or xenograft-derived cells were dissociated as single cells, washed with PBS and incubated with the appropriate dilutions of control or specific antibodies for 45 min at room temperature. Fluorescence intensity of labeled cells was evaluated with a FACS Canto (BD Biosciences). 7-Aminoactinomycin D (10 μ g/ml; 7-AAD; Sigma-Aldrich) was added for dead cell exclusion. For the detection of intracellular antigens, cells were fixed in 2% paraformaldehyde and permeabilized in 0.1% Triton X-100 (Bio-Rad Laboratories) and then incubated 45 min at room temperature with primary antibodies dissolved in PBS 1% BSA. After being washed in PBS, cells were incubated with AlexaFluor-647 secondary antibodies for 30 min at room temperature in the dark.

Immunofluorescence analysis of cultured cells and xenograft sections. LCSC spheroids or dissociated cells were cytospun on polylysine-coated glass slides, whereas differentiated cells were grown on matrigel-coated coverslips. Cells were fixed in 2% paraformaldehyde and permeabilized in 0.1% Triton X-100 and then incubated overnight at 4 °C with primary antibodies dissolved in PBS 3% BSA. After being washed in PBS, cells were incubated with Alexa Fluor-conjugated secondary antibodies for 45 min at room temperature in the dark, stained for 15 min with Dapi (Invitrogen) diluted in PBS 3% BSA and mounted with Prolong-Gold antifade (Invitrogen). Negative controls were prepared by omitting staining with the primary antibody. To determine mitochondrial membrane potential in live cells, LCSC spheroids were incubated for 1 h at 37 °C with 10 μ M JC-1 (Invitrogen). Cytochrome c and AIF release from mitochondria were determined by staining live cells for 30 min at 37 °C with 100 nM Mitotracker CMXRos (Invitrogen). Cells were then fixed, permeabilized and incubated with the respective monoclonal antibodies as described above. Tumor xenografts previously embedded in optimal cutting temperature compound (OCT) and frozen at -80 °C were cut into 5- μ m-thick tumor sections with a cryomicrotome (Kriostat 1720 MGW Leitz, Melville, NY, USA). Sections were fixed in 4% paraformaldehyde and permeabilized in 0.1% Triton X-100, then stained overnight at 4 °C with primary antibodies, incubated with fluorochrome-conjugated secondary antibodies and counterstained with Dapi. For *in situ* apoptosis detection in tumor xenograft sections, TUNEL reaction was performed using the *In situ* Cell Death Detection kit (Roche Molecular Biochemicals) according to the manufacturer's instructions. Slides were analyzed using an Olympus FV-1000 confocal microscope equipped with Ultraplano Apochromatic $\times 60$ N.A.1.35 and $\times 40$ N.A. objectives and the Olympus Fluoview software (Olympus, Tokyo, Japan).

Mice treatment. All animal procedures were performed according to the national Animal Experimentation guidelines (D.L.116/92) upon approval of the experimental protocol by the Institutional Animal Experimentation Committee. Female 6–8 weeks old NOD.Cg-Prkdcscid Il2rgtm1Wj/SzJ (NSG) mice (The Jackson Laboratory, Bar Harbor, ME, USA) were subcutaneously injected with 5×10^5 cells resuspended in 100 μ l Matrigel/LCSC medium (1:1). Mice were kept under pathogen-free conditions with food and water *ad libitum*. Tumor diameter was measured by using an external digital caliper and calculated as the mean value between the shortest and the longest diameters. When tumor diameters reached an

approximate volume of 200–250 mm³, the treatment was started. The control group ($n=6$) was treated daily by injecting intraperitoneally (i.p.) a vehicle solution composed of 100 μ l of 30% PEG, 5% Tween 80 and 65% D5W (5% dextrose in water) at pH 4–4.5. The ABT-737 group ($n=6$) was treated by injecting i.p. the compound daily (100 mg/kg) dissolved in vehicle solution. The chemotherapy group ($n=6$) was treated by injecting i.p. gemcitabine (60 mg/kg) resuspended in PBS twice a week. Three weeks after the beginning of treatment, the mice were killed by cervical dislocation and tumors were removed, weighted and processed for flow cytometry analysis. For analysis of DNA fragmentation (TUNEL), PARP or caspase-3 cleavage, a short-term treatment with ABT-737 was performed by injecting i.p. the vehicle solution, ABT-737 150 mg/kg or gemcitabine 100 mg/kg. Forty-eight hours after treatment mice were killed and tumors were removed, embedded in OCT and frozen at -80 °C for subsequent immunofluorescence analysis.

Statistical analysis. The statistical significance of the results was evaluated by ANOVA and Bonferroni post tests. All statistical tests were performed using GraphPad Prism v.4.0 for Windows (GraphPad Software, San Diego, CA, USA, www.graphpad.com) and the threshold for statistical significance was set at 0.05. *P*-values are displayed on the graphs using a single asterisk for significances ranging from 0.05 to 0.01, two asterisks for values between 0.001 and 0.01 and three asterisks for values below 0.001.

Conflict of Interest

The authors declare no conflict of interest.

Acknowledgements. This work was supported by the Associazione Italiana per la Ricerca sul Cancro (AIRC) grant 'Molecular Oncology 5 x Mille Program' to RDM. We thank Stefano Guida (Istituto Superiore di Sanità, ISS) for excellent technical assistance, Alessandra Boe (ISS) for flow cytometry assistance, Giuseppe Loreto (ISS) for graphics, Emanuela Pillozzi (S. Andrea Hospital, Rome) for providing NSCLC tumor samples, Donatella Pietraforte (ISS) for providing radical scavengers and advice, Ilio Vitale (Regina Elena National Cancer Institute, Rome) for helpful discussion, Tobias L. Haas (Regina Elena National Cancer Institute, Rome) and Henning Walczak (Imperial College, London) for providing TNF- α and LZ-TRAIL.

Author contributions

Author contributions GZ, FF, MT, TA and PC performed experiments, MBa and MLDA provided essential support with animal experiments, MBI was responsible for flow cytometry analysis, GSe and AE produced the LCSC lines, GSt and RDM supervised the study, AZ wrote the manuscript, designed and supervised the experiments.

- Jemal A, Bray F, Center MM, Ferlay J, Ward E, Forman D. Global cancer statistics. *CA: a cancer journal for clinicians* 2011; **61**: 69–90.
- Malvezzi M, Arfe A, Bertuccio P, Levi F, La Vecchia C, Negri E. European cancer mortality predictions for the year 2011. *Ann Oncol* 2011; **22**: 947–956.
- Eramo A, Haas T, De Maria R. Lung cancer stem cells: tools and targets to fight lung cancer. *Oncogene* 2010; **29**: 4625–4635.
- Eramo A, Lotti F, Sette G, Pillozzi E, Biffoni M, Di Virgilio A *et al*. Identification and expansion of the tumorigenic lung cancer stem cell population. *Cell Death Differ* 2007; **15**: 504–514.
- Levina V, Marrangoni A, Wang T, Parikh S, Su Y, Herberman R *et al*. Elimination of human lung cancer stem cells through targeting of the stem cell factor-c-kit autocrine signaling loop. *Cancer Res* 2010; **70**: 338–346.
- Levina V, Marrangoni AM, DeMarco R, Gorelik E, Lokshin AE. Drug-selected human lung cancer stem cells: cytokine network, tumorigenic and metastatic properties. *PLoS One* 2008; **3**: e3077.
- Jiang F, Qiu Q, Khanna A, Todd NW, Deepak J, Xing L *et al*. Aldehyde dehydrogenase 1 is a tumor stem cell-associated marker in lung cancer. *Mol Cancer Res* 2009; **7**: 330–338.
- Zhang WC, Shyh-Chang N, Yang H, Rai A, Umashankar S, Ma S *et al*. Glycine decarboxylase activity drives non-small cell lung cancer tumor-initiating cells and tumorigenesis. *Cell* 2012; **148**: 259–272.
- Ye XQ, Li Q, Wang GH, Sun FF, Huang GJ, Bian XW *et al*. Mitochondrial and energy metabolism-related properties as novel indicators of lung cancer stem cells. *Int J Cancer* 2011; **129**: 820–831.
- Baiocchi M, Biffoni M, Ricci-Vitiani L, Pillozzi E, De Maria R. New models for cancer research: human cancer stem cell xenografts. *Curr Opin Pharmacol* 2010; **10**: 380.
- Kelly PN, Strasser A. The role of Bcl-2 and its pro-survival relatives in tumorigenesis and cancer therapy. *Cell Death Differ* 2011; **18**: 1414–1424.

12. Davids MS, Letai A. Targeting the B-cell lymphoma/leukemia 2 family in cancer. *J Clin Oncol* 2012; **30**: 3127–3135.
13. Lagadinou ED, Sach A, Callahan K, Rossi RM, Neering SJ, Minhajuddin M *et al*. BCL-2 inhibition targets oxidative phosphorylation and selectively eradicates quiescent human leukemia stem cells. *Cell Stem Cell* 2013; **12**: 329–341.
14. Goff DJ, Sadarangani A, Chun H-J, Barrett CL, Krajewska M, Leu H *et al*. A Pan-BCL2 inhibitor renders bone-marrow-resident human leukemia stem cells sensitive to tyrosine kinase inhibition. *Cell Stem Cell* 2013; **12**: 316–328.
15. Akunuru S, Zhai QJ, Zheng Y. Non-small cell lung cancer stem/progenitor cells are enriched in multiple distinct phenotypic subpopulations and exhibit plasticity. *Cell Death Dis* 2012; **3**: e352.
16. Bartucci M, Svensson S, Romania P, Dattilo R, Patrizii M, Signore M *et al*. Therapeutic targeting of Chk1 in NSCLC stem cells during chemotherapy. *Cell Death Differ* 2011; **19**: 768–778.
17. Gao M, Choi Y, Kang S, Youn J, Cho N. CD24⁺ cells from hierarchically organized ovarian cancer are enriched in cancer stem cells. *Oncogene* 2010; **29**: 2672–2680.
18. Pece S, Tosoni D, Confalonieri S, Mazzarol G, Vecchi M, Ronzoni S *et al*. Biological and molecular heterogeneity of breast cancers correlates with their cancer stem cell content. *Cell* 2010; **140**: 62–73.
19. Roesch A, Fukunaga-Kalabis M, Schmidt EC, Zabierowski SE, Brafford PA, Vultur A *et al*. A temporarily distinct subpopulation of slow-cycling melanoma cells is required for continuous tumor growth. *Cell* 2010; **141**: 583–594.
20. Dembinski JL, Krauss S. Characterization and functional analysis of a slow cycling stem cell-like subpopulation in pancreas adenocarcinoma. *Clinical Exp Metastasis* 2009; **26**: 611–623.
21. Francescangeli F, Patrizii M, Signore M, Federici G, Di Franco S, Pagliuca A *et al*. Proliferation state and polo-like kinase1 dependence of tumorigenic colon cancer cells. *Stem Cells* 2012; **30**: 1819–1830.
22. Moore N, Lyle S. Quiescent, slow-cycling stem cell populations in cancer: a review of the evidence and discussion of significance. *J Oncol* 2010; **2011**: 396076.
23. Martinou J-C, Youle RJ. Mitochondria in apoptosis: Bcl-2 family members and mitochondrial dynamics. *Dev Cell* 2011; **21**: 92–101.
24. Visvader JE, Lindeman GJ. Cancer stem cells: current status and evolving complexities. *Cell Stem Cell* 2012; **10**: 717–728.
25. Chen J, Li Y, Yu T-S, McKay RM, Burns DK, Kernie SG *et al*. A restricted cell population propagates glioblastoma growth after chemotherapy. *Nature* 2012; **488**: 522–526.
26. Oltsersdorf T, Elmore SW, Shoemaker AR, Armstrong RC, Augeri DJ, Belli BA *et al*. An inhibitor of Bcl-2 family proteins induces regression of solid tumours. *Nature* 2005; **435**: 677–681.
27. Wesarg E, Hoffarth S, Wiewrodt R, Kröll M, Biesterfeld S, Huber C *et al*. Targeting BCL-2 family proteins to overcome drug resistance in non-small cell lung cancer. *Int J Cancer* 2007; **121**: 2387–2394.
28. Fan W, Tang Z, Yin L, Morrison B, Hafez-Khayyata S, Fu P *et al*. MET-independent lung cancer cells evading EGFR kinase inhibitors are therapeutically susceptible to BH3 mimetic agents. *Cancer Res* 2011; **71**: 4494–4505.
29. Juin P, Geneste O, Gautier F, Depil S, Campone M. Decoding and unlocking the BCL-2 dependency of cancer cells. *Nat Rev Cancer* 2013; **13**: 455–465.
30. Zhang H, Nimmer P, Tahir S, Chen J, Fryer R, Hahn K *et al*. Bcl-2 family proteins are essential for platelet survival. *Cell Death Differ* 2007; **14**: 943–951.
31. Song JH, Kandasamy K, Zemskova M, Lin Y-W, Kraft AS. The BH3 mimetic ABT-737 induces cancer cell senescence. *Cancer Res* 2011; **71**: 506–515.
32. Howard AN, Bridges KA, Meyn RE, Chandra J. ABT-737, a BH3 mimetic, induces glutathione depletion and oxidative stress. *Cancer Chemother Pharmacol* 2009; **65**: 41–54.
33. Diehn M, Cho RW, Lobo NA, Kalisky T, Dorie MJ, Kulp AN *et al*. Association of reactive oxygen species levels and radioresistance in cancer stem cells. *Nature* 2009; **458**: 780–783.
34. Haas TL, Emmerich CH, Gerlach B, Schmukle AC, Cordier SM, Rieser E *et al*. Recruitment of the linear ubiquitin chain assembly complex stabilizes the TNF-R1 signaling complex and is required for TNF-mediated gene induction. *Mol Cell* 2009; **36**: 831–844.
35. Enyedy IJ, Ling Y, Nacro K, Tomita Y, Wu X, Cao Y *et al*. Discovery of small-molecule inhibitors of Bcl-2 through structure-based computer screening. *J Med Chem* 2001; **44**: 4313–4324.
36. Ewald JA, Desotelle JA, Wilding G, Jarrard DF. Therapy-induced senescence in cancer. *J Natl Cancer Inst* 2010; **102**: 1536–1546.

Supplementary Information accompanies this paper on Cell Death and Differentiation website (<http://www.nature.com/cdd>)